Characterization of peroxyacetyl nitrate (PAN) under different PM2.5 concentration in wintertime at a North China rural site

Zhuoyu Li, Guangzhao Xie, Hui Chen, Bixin Zhan, Lin Wang, Yujing Mu, Abdelwahid Mellouki, Jianmin Chen

Characterization of peroxyacetyl nitrate (PAN) under different $PM_{2.5}$ concentration in wintertime at a North China rural site

Zhuoyu Li[1], Guangzhao Xie[1], Hui Chen[1], Bixin Zhan[1], Lin Wang[1], Yujing Mu[2,3], Abdelwahid Mellouki[4], Jianmin Chen[1,2,3,*]

[1]Department of Environmental Science & Engineering, Fudan Tyndall Center, Institute of Atmospheric Sciences, Fudan University, Shanghai 200438, China

[2]Center for Excellence in Regional Atmospheric Environment, Institute of Urban Environment, Chinese Academy of Sciences, Xiamen 361021, China.

[3]Research Center for Eco-Environmental Sciences, Chinese Academy of Sciences, Beijing 100085, China.

[4]Institut de Combustion, Aérothermique, Réactivité et Environnement, Centre National de la Recherche Scientifique, 45071 Orléans cedex 02, France

Abstract

As a secondary pollutant of photochemical pollution, peroxyacetyl nitrate (PAN) has attracted a close attention. A four-month campaign was conducted at a rural site in North China Plain (NCP) including the measurement of PAN, O_3, NO_x, $PM_{2.5}$, oxygenated volatile organic compounds (OVOCs), photolysis rate constants of NO_2 and O_3 and meteorological parameters to investigate the wintertime characterization of photochemistry from November 2018 to February 2019. The results showed that the maximum and mean values of PAN were 4.38 and 0.93 ± 0.67 ppbv during the campaign, respectively. The PAN under different $PM_{2.5}$ concentrations from below 75 μg/m^3 up to 250 μg/m^3, showed different diurnal variation and formation rate. In the $PM_{2.5}$ concentration range of above 250 μg/m^3, PAN had the largest daily mean value of 0.64 ppbv and the fastest production rate of 0.33 ppbv/hr. From the perspective of PAN's production mechanism, the light intensity and precursors concentrations under different $PM_{2.5}$ pollution levels indicated that there were sufficient light intensity and high volatile organic compounds (VOCs) and NO_x precursors concentration even under severe pollution level to generate a large amount of PAN. Moreover, the bimodal staggering phenomenon of PAN and $PM_{2.5}$ provided a basis that PAN might aggravate haze through secondary organic aerosols (SOA) formation.

Keywords:

Peroxyacetyl nitrate

$PM_{2.5}$

Wintertime

North China

Rural site

---

*Corresponding author. E-mail: jmchen@fudan.edu.cn (Jianmin Chen)

Introduction

Peroxyacetyl nitrate (PAN) is an important photochemical oxidation product, which exists widely in the tropospheric atmosphere. PAN was first discovered in the photochemical smog of Los Angeles in 1956 by Stephens et al. (1956). Related studies have pointed out that PAN can cause severe irritation to human eyes and may even cause skin mutations. PAN is approximately two times more irritating than formaldehyde. In addition, it can produce injury on plant leaves such as tomato plants (Altshuller, 1978; Carter et al., 1981; Taylor, 1969).

PAN has no natural source and can be produced exclusively by the reactions of volatile organic compounds (VOCs) and NO_2 (Aikin et al., 1982; LaFranchi et al., 2010). Acetaldehyde is the main precursor of PAN (Kondo et al., 2008). In addition, acetone, methacrolein (MACR), methylglyoxal (MGLY), methyl ethyl ketone (MEK), methyl vinyl ketone (MVK), biacetyl are also the precursors of PAN. Most of these compounds are second-generation precursors. Among the first-generation precursors that produce OVOCs, aromatics and isoprene are the most contributors (Xue et al., 2014). These VOCs can generate peroxyacetyl (PA) radicals through photolysis or oxidation by OH or NO_3 and then PA radicals react with NO_2 to produce PAN. Thermal decomposition accounts for a large fraction degradation of PAN. The lifetime of PAN is only 35 min at 298 K, but at 247 K, it can be as long as 5 years (Atkinson et al., 1997; Atkinson et al., 1992). Through thermal degradation, PAN can release PA radicals and NO_2, therefore PAN is considered as a reservoir of NO_x. Meanwhile PAN becomes a precursor for formaldehyde and free radicals (Orlando et al., 1992; Singh et al., 1986). With low temperature stability, PAN can be transported to distant places in winter or at the top of troposphere thereby affecting regional atmospheric chemistry (Honrath et al., 1996; Roberts et al., 2004). Besides, PAN can also be removed by photolysis, reaction with OH radicals, and wet

or dry deposition.

In recent years, a large number of PAN observations experiments have continued to be carried out over the world. Observation sites have covered large cities, suburbs, rural areas, seaside areas, and even polar regions (Singh and Salas, 1983). The observed PAN concentrations ranged from a few pptv in inaccessible places to 30 ppbv in megacities (Gaffney et al., 1999; Jacobi et al., 1999; Mills et al., 2007). The atmospheric environment of different sites determined the pollution characteristics of PAN, which provided data basis for comparison and analysis between different regions. Photochemical pollution in China has also received more and more attention, and PAN has been measured in some places of China such as Beijing, Lanzhou (Zhang et al., 2014, 2009). Blanks about characteristics of PAN in more regions need to be filled. Many literatures have focused on the relationship of PAN and O_3. The correlation analysis of PAN and O_3 also has obvious differences in seasons or regions. In general, there is a positive correlation between PAN and O_3. However, there are less research that focus on the relationship between PAN and $PM_{2.5}$. Unlike what is known in theory, high concentrations of $PM_{2.5}$ are usually accompanied by an increase in PAN concentrations. Many studies have noted positive correlation between PAN and $PM_{2.5}$, but correlation analysis can provide weak evidence. Zhao et al. (2017) simulated the heterogeneous reaction of PAN on soot surface, which suggested the link between PAN and particulate matter (PM). Especially in winter, the relationship between severe haze pollution and the formation and sink mechanism of PAN become more complicated. Laboratory research has also constantly been conducted on the heterogeneous reactions of PAN i.e., liquid phase reaction, particle surface reaction (Frenzel et al., 2000; Langer et al., 1992). However, the complex atmospheric environment makes the research between PAN and $PM_{2.5}$ difficult.

In this study, we conducted measurements of PAN, $PM_{2.5}$, trace gas, meteorological data and photolysis rate constants from Nov. 2018 to Feb. 2019 in Wangdu of Hebei Province to provide better understanding photochemical pollution in our country's rural areas. This observation filled the scarcity of PAN in rural areas. We analyzed the characterization of PAN under different pollution conditions characterized by concentrations of $PM_{2.5}$. From the perspective of PAN-producing precursors, the reasons for the elevation in PAN concentrations in severe pollution periods were analyzed. Additionally, the effect of PAN on $PM_{2.5}$ was studied during the periods when the PAN

concentrations exceeded 2 ppbv.

1. Material and methods

1.1. Measurement site

Field measurement was carried out from November 2018 to February 2019 in Wangdu (115.12° E, 38.40°N), which located in the central area of the Beijing-Tianjin-Shijiazhuang region. Wangdu County is ~90 km south to Shijiazhuang, ~35 km north to Baoding, and ~180 km north to Beijing. There is 230,000 agricultural population. Our site is ~1 km northwest to a 8-lane highway (G4) and surrounded by farmland and villages. As a heavily polluted rural area, Wangdu observation is necessary and significant.

1.2. Measurement techniques

PAN concentrations were detected by online system using a gas chromatograph equipped with an electron capture detector (GC-ECD, PANs-1000, Focused Photonics Inc., Hangzhou, China). The working principle of the system was as follows: when start sampling, the sample entered the quantitative loop after being filtered through the polytetrafluoroethylene (PTFE) microporous filter membrane. After that, the sample was separated in chromatographic column. The separated components were brought into the electron capture detector (ECD) for detection, and the output electrical signal was recorded. The detection limit of analyzer (PANs-100, Focused Photonics Inc., Hangzhou, China) was 50 pptv. The uncertainty and precision were up to 10% and 3%, respectively. The calibration system (PANs-200, Focused Photonics Inc., Hangzhou, China) consisted of a flow control unit, a synthesis reaction unit, and a dilution mixing unit. The flow control unit controlled the flow of NO, acetone and zero air to achieve precise control of reactant gas. The synthesis reaction unit was composed of a reaction chamber, an ultraviolet lamp and a radiator fan. After acetone (20 ppmv) and NO (1 ppmv) standard gas were mixed, the ultraviolet light penetrated the wall of the reaction chamber to irradiate mixed gas for photochemical synthesis reaction. The dilution mixing unit diluted the PAN synthesized by acetone and NO through zero air to obtain the target concentration. In addition to diluting the PAN standard gas, zero air also provided a PAN-free baseline. The multi-point calibration was conducted once a month, and the single-point calibration was conducted once a week.

A series of supporting information including NO_x/NO/NO_2, CO, O_3 were measured by

monitors (42i, 48i, 49i, Thermo Scientific Inc., MA, USA). The calibration was performed by the gaseous analyzer every 5 days. Meteorological parameters (wind speed, wind direction) were obtained by an automatic weather station (Vaisala, Helsinki, Finland). The concentrations of $PM_{2.5}$ were gained by using the Synchronized Hybrid Ambient Real-time Particulate Monitor (Sharp Model 5030i, Thermo Scientific Inc., MA, USA), with a time resolution of 1 hr.

Online oxygenated VOCs (OVOCs) measurement was obtained by using gas chromatography–mass spectrometry detector (GC–MS, ZF-PKU-VOC1007, Pengyuchangya Inc., Beijing, China) with a time resolution of 1 hr. A total of 13 OVOCs were identified and quantified. The air samples were first enriched in a capillary column (15 cm × 0.53 mm inner diameter (ID)), and then transferred into the GC-MS channel to be measured with a DB-624 column (60 m × 0.25 mm ID). The detection limit of OVOCs varied from 0.001 to 0.015 ppbv. The photolysis rate constants of NO_2, O_3 were detected by photolysis spectrometer (PFS-100, Focused Photonics Inc., Hangzhou, China) which mainly used quartz receiver to collect solar radiation from all directions, then the signal scanned by the spectrometer was converted into photochemical flux (F_λ) to calculate photolysis rate constants. The instrument had simple structure and fast response speed, and could obtain the photolysis rate of important substances and free radicals in the atmosphere in real time.

1.3. Net formation rate

The net formation rate for PAN, O_x is defined in Eq. (1)

$$\text{Net formation rate (ppbv/hr)} = \frac{C_{t+1} - C_t}{1\ \text{hour}} \qquad (1)$$

where C represents the concentrations of PAN or O_x at a certain moment, and t is the time. To exclude the effect of mixing layer height, we use CO-scaled rate to further illustrate the chemical processes.

The calculation is as follows:

$$\text{Net CO-scaled formation rate (ppbv/hr)} = \frac{(C/\text{CO})_{t+1} - (C/\text{CO})_t}{1\ \text{hour}} \qquad (2)$$

where C/CO represents the concentrations of PAN or O_x divided by CO.

2. Results and discussion

2.1. Time series and overviews of PAN

We conducted observations of PAN, $PM_{2.5}$, O_3, NO, NO_2, VOCs and meteorological

parameters from November 2018 to February 2019 at Wangdu. The time series of above pollutants are showed in Fig. 1. The mass concentrations of $PM_{2.5}$ ranged from 0.93 to 823 μg/m^3 with an average of 184.13 ± 138.32 μg/m^3, which reflected the severe haze pollution level in rural areas of the North China Plain (NCP). High concentrations of particulate matter (PM) in the NCP were often reported (Liu et al., 2017; Xu et al., 2019). The maximum and mean values of PAN were 4.38 and 0.93 ± 0.67 ppbv. Table 1 presents previous observation data of PAN for comparison. Compared with observations values of other sites during winter, the values of PAN in Wangdu were at a higher level. They were higher than those such as in Beijing (maximum: 1.46 ppbv, mean: 0.31 ppbv) during November 2012 - January 2013, in Ziyang (maximum: 1.61 ppbv, mean: 0.55 ppbv) during Dec. 2012, in Xiamen (maximum: 4.19 ppbv, mean: 0.64 ppbv) during December 2016 - January 2017. Of course, higher concentrations of PAN have been reported in the literature. Liu et al. (2018) reported quite high values of PAN during winter in Jinan (maximum: 9.61 ppbv, mean: 1.89±1.42 ppbv) due to high local formation. In history, the highest record of PAN concentration was in Mexico in 1997, which reached 34 ppbv.

Generally, the concentrations of PAN are higher in summer than in winter which is because stronger photochemical reaction in summer can produce a large amount of PAN. However, the concentrations of PAN during winter in Wangdu even were at a comparable level in summer in some places. Judging from the location of the sites, the PAN concentrations in urban areas are usually higher than in rural areas due to more anthropogenic emission sources in urban areas. However, located in rural areas, the concentrations of PAN in Wangdu are at a higher level than other rural sites, and even higher than that in some urban areas, indicating that Wangdu had serious photochemical pollution in winter.

2.2. Characteristics of PAN under different concentrations of $PM_{2.5}$

2.2.1. Diurnal variation

According to the second-grade Chinese National Ambient Air Quality Standard (CNAAQS), the concentrations of $PM_{2.5}$ were divided into four levels. In order to illustrate the differences in characteristics of pollutants under different pollution conditions, we classified the measurement days into four categories (<75 μg/m^3, 75-150 μg/m^3, 150-250 μg/m^3, and > 250 μg/m^3) according to different $PM_{2.5}$ concentrations. In order from low to high, these four levels represented clean periods, light haze pollution, moderate haze pollution, and severe haze pollution. The days in these

four ranges respectively accounted for 14.3%, 25%, 37.5%, 23.2% of the total observation days which illustrated severe haze pollution. Note that all values were under stable weather (wind speed $<$2 m/sec). The mean diurnal profiles of PAN, O_3, O_x, NO, NO_2 which were calibrated with CO are illustrated in Fig. 2. CO is hard to react with other pollutants in atmosphere due to its inertness and CO concentrations mainly controlled by meteorological factor. To understand the influence of chemical processes to pollution concentrations, CO ratios method is always used to exclude dilution effects and calculate the chemical growth rate (Kuang et al., 2020; Liu et al., 2019). Zhang et al. (2015) considered CO as a tracer and used the ratios of SO_2/CO, NO_x/CO, and O_3/CO.

Generally, the early morning rise in CO-scaled PAN concentrations happened from 8:00 local time (LT) which were consistent with the beginning of acute photochemical reactions. CO-scaled PAN reached its maximum value at 15:00 LT under the $PM_{2.5}$ concentrations range of 75-150, 150-250, and above 250 μg/m^3, one hour later than the periods of below 75 μg/m^3. Different haze pollution levels had a relatively small impact on the time for CO-scaled PAN to appear its maximum value. As the pollution level increased, the daily average maximum values of CO-scaled PAN presented a trend of increasing first, then decreasing and then increasing. During the periods of 75-150 μg/m^3, the daily maximum of CO-scaled PAN was the highest with the value of 1.52 ppbv. When the concentrations of $PM_{2.5}$ exceeded 250 μg/m^3, the average CO-scaled PAN concentration increased continuously from 0.23 ppbv at 8:00 LT to 1.39 ppbv at 15:00 LT. And during the daytime, the concentrations of PAN were the highest during some periods. Overall PAN had the largest daily mean value of 0.64 ppbv when $PM_{2.5}$ concentrations exceeded 250 μg/m^3. Compared with clean periods, PAN concentrations in the haze periods were significantly higher. O_3 and PAN were both products of photochemical reactions, so their diurnal changes were similar. Generally CO-scaled O_3 presented unimodal change, which increased from 8:00 LT to 15:00 LT when $PM_{2.5}$ exceeded 75 μg/m^3. For below 75 μg/m^3 concentrations, CO-scaled O_3 peaked at 14:00 LT. Different from CO-scaled PAN, the maximum values of CO-scaled O_3 gradually decreased with the aggravation of pollution, which showed that formation and accumulation of O_3 was suppressed in highly polluted condition. Considering the titration of NO, we further researched on the diurnal variation of odd oxygen ($O_x = O_3 + NO_2$). The time for O_x to reach its maximum values was the same as that of O_3. The difference was that although the concentrations of CO-scaled O_x showed downward trend as pollution worsened, when $PM_{2.5}$ exceeded 250 μg/m^3, it increased, implying that atmospheric oxidizing ability during heavy haze periods enhanced. CO-scaled NO presented unique bimodal change, which accumulated to peak at midnight and decreased before dawn, then due to motor

vehicle exhaust emissions reached the peak at 8:00 LT. As the photochemical precursors, NO rapidly participated in the photochemical reaction under strong solar radiation which led to decline after 8:00 LT and then increased from 16:00 LT. When $PM_{2.5}$ concentrations were between 75 and 150 $\mu g/m^3$, concentrations of CO-scaled NO were the lowest, which might be the reason for the highest daily maximum of PAN during this period. As competitive reaction of PAN formation, NO could react with peroxyacetyl (PA) radicals which led to generate fewer PAN. In general, there was little difference in NO concentrations during the daytime. Due to the conversion of NO, the concentrations of CO-scaled NO_2 began to rise from 8:00 LT, and arrived maximum values between 15:00 LT and 17:00 LT. When $PM_{2.5}$ concentrations were between 75 and 150 $\mu g/m^3$, the daily maximum of NO_2 was the largest. As the pollution worsened, although the maximum daily value decreased, other daytime hours were not much different or even the concentrations increased.

2.2.2. Formation rate

To further analyze the behaviors of PAN under different $PM_{2.5}$ concentrations, net formation rate of PAN and CO-scaled PAN, O_x were illustrated in Fig. 3. The divergence in the formation rate of PAN before and after correction was obvious, indicating boundary layer had a certain influence on the concentrations. Except periods of severe pollution (>250 $\mu g/m^3$), net formation rate of CO-scaled PAN all appeared in the afternoon (13:00 LT or 14:00 LT). During heavy pollution periods, the peak of net CO-scaled formation rate advanced to 10:00 LT with maximum value of 0.33 ppbv/hr. The atmospheric environment at that time determined net formation rate of CO-scaled PAN. The reason for the maximum generation rate time point in advance during conditions of above 250 $\mu g/m^3$ requires more relevant data to explain in the future. As the pollution level deepened, the net CO-scaled formation rate of PAN presented a trend of rising first, then falling, and then rising again. When concentrations of $PM_{2.5}$ exceeded 250 $\mu g/m^3$, net formation rate of CO-scaled PAN during the daytime was significantly accelerated. PAN still kept a rapid formation rate during the heavy pollution periods. According to the daily variation and net formation rate of PAN under different levels of $PM_{2.5}$, we can speculate that during severe haze periods, it is favorable for the formation of PAN which will be explored in detail in next section. For lower $PM_{2.5}$ concentrations, net formation rate of CO-scaled O_x was the highest with average daily maximum of 39.29 ppbv/hr. When $PM_{2.5}$ concentrations were below 250 $\mu g/m^3$, maximum value also appeared at 14:00 LT. When $PM_{2.5}$ concentrations exceeded 250 $\mu g/m^3$, maximum values appeared before noon. The high

$PM_{2.5}$ concentrations inhibited the formation rate of CO-scaled O_x to a certain extent. During heavy haze periods, PAN and O_x presented different growth characteristics. In summary, diurnal profile and considerable formation rate of PAN and O_x indicated higher photochemical reaction intensity under high $PM_{2.5}$ concentrations.

2.3. PAN and its precursors

The reaction process indicates the formation of PAN is affected by the concentrates of precursors (VOCs, NO_x), solar intensity and temperature. PAN is formed through the reaction of VOCs and NO_2. VOCs are oxidized by OH radicals or photodegraded to generate PA radicals. And then, PA radicals react with NO_2 to produce PAN. PAN can be removed through thermal degradation to release PA radicals and NO_2. In addition to reacting with NO_2, PA radicals can also be reduced to acetoxy by NO. The reaction formula is as follows:

$$VOCs + OH/h\nu \rightarrow CH_3C(O)OO + products \quad (3)$$

$$CH_3C(O)OO + NO_2 \rightarrow CH_3C(O)OONO_2 \quad (4)$$

$$CH_3C(O)OONO_2 \rightarrow CH_3C(O)OO + NO_2 \quad (5)$$

$$CH_3C(O)OO + NO \rightarrow CH_3C(O)O + NO_2 \quad (6)$$

where *hv* is irradiation with light.

As shown in Reaction (5), thermal decomposition is a prominent removal pathway of PAN, which is mainly affected by temperature. Compared with summer, the lifetime of PAN in winter increase significantly. Considering only thermal decomposition, the lifetime of PAN in winter can be calculated with the following formula:

$$\tau\,(PAN) = \frac{1}{k_3}\left(1+\frac{k_2[NO_2]}{k_4[NO]}\right) \quad (7)$$

where τ (PAN) (sec) represents the lifetime of PAN; k_2 (cm^3/(molecule·sec)) is the rate constant for Reaction (4); k_3 (sec^{-1}) is the rate constant for Reaction (5); and k_4 (cm^3/(molecule·sec)) is the rate constant for Reaction (6).

According to the formula, the lifetime of PAN was related to temperature and the ratio of NO_2 to NO, so we calculated the lifetime of PAN for three conditions distinguished by $PM_{2.5}$ concentrations: clean days (<75 μg/m^3), moderate haze days (75-250 μg/m^3), severe haze days (>250 μg/m^3). Table 2 shows the lifetime of PAN in three conditions. The temperature and ratio of NO_2 to NO involved in the calculation were calculated using average values. In winter, the

temperature was around 273 K on average in Wangdu, which was in favor of the accumulation of PAN. There was a big difference in the ratio of NO_2 to NO. The lifetime of PAN in the three conditions was 80, 10, and 5 days respectively. There was lower lifetime of PAN during severe haze episodes due to lower ratio of NO_2 to NO. The significantly reduced lifetime of PAN in the haze period indicated that compared with clean episodes, there was faster photochemical reaction rate in haze episodes, especially in severe haze episodes. This phenomenon was consistent with the above findings.

Theoretically, high concentrations of PM will weaken the solar light and inhibit the generation of PAN. Contrary to theory, elevated PAN concentrations are frequently accompanied with increasing levels of $PM_{2.5}$ during winter in this study. According to the formation mechanism we used the photolysis rate constants of NO_2 and O_3 (JNO_2 and JO^1D) to reflect the solar radiation intensity near the ground. The photolysis reaction of O_3 is mainly affected by wavelengths below 330 nm (Casasanta et al., 2011), while NO_2 is mainly affected by wavelengths shorter than 410 nm (Atkinson et al., 2004). Moreover, the formation of PAN need oxidants which can be generated by the photolysis of O_3. The photolysis of NO_2 can influence atmospheric oxidation and photochemical pollution process. Therefore, the combination of JNO_2 and JO^1D can better reflect the light radiation intensity of the wave involved in the photochemical reaction. Fig. 4 shows diurnal variation in the photolysis rate constants of NO_2 and O_3 divided according to different concentrations of $PM_{2.5}$. For JNO_2, high particle concentrations didn't obviously have an unfavorable effect on the intensity of photolysis rate constants. Even under extremely high $PM_{2.5}$ concentrations, JNO_2 exceeded that of clean episodes for a few days, which probably resulted from the different interference ability of diverse particle sizes to different wavelengths of light. For JO^1D, when $PM_{2.5}$ exceeded 75 $\mu g/m^3$, photolysis rate constants decreased significantly. High concentrations of $PM_{2.5}$ inhibited the photolysis of O_3, consistent with the fact that photolysis of O_3 under haze periods was not the main way to produce OH radicals (Fuchs et al., 2017; Lu et al., 2013). Combined with the variation of JNO_2 and JO^1D, we inferred there was still moderate light radiation intensity in high $PM_{2.5}$ concentrations, which was very likely to be one of the reasons for elevated photochemical reaction rate to generate PAN at Wangdu during severe haze pollution periods.

Although the photolysis rate of O_3 decreased during high $PM_{2.5}$ concentrations, studies have shown that HONO is the main source of OH radicals during haze pollution period in winter (Bao et al., 2018). Regrettably, we lacked the data of HONO in this observation. Liu et al. (2014) found that aerosols played an important role on daytime heterogeneous HONO formation. And Zhang et al. (2019) measured that the formation rate of OH radicals through the photolysis of HONO and the loss rate of OH radicals through reaction with VOCs were enhanced on haze days compared with non-haze days at Wangdu site over winter observation campaign in 2017. It could be seen that HONO produced enough OH radicals to participate in the photochemical reaction at Wangdu during winter.

It has become a recognized fact that the concentrations of VOCs increase during pollution periods (Liu et al., 2017; Sun et al., 2016). Primary emitted VOCs are transformed to OVOCs by OH radicals, so we mainly focus on OVOCs in this study. The 3D scatter plot of precursors (OVOCs, NO_2) and PAN divided according to $PM_{2.5}$ concentrations is shown in Fig. 5a. In order to show more clearly, the PAN and precursors concentrations in the four grade ranges are also shown in the four graphs. In general, the concentrations of CO-scaled OVOCs and NO_2 were lower when $PM_{2.5}$ concentrations were below 75 $\mu g/m^3$, which was consistent with less PAN in clean periods. Under clean periods, when the concentrations of CO-scaled NO_2 were between 10 and 30 ppbv, as the concentrations of CO-scaled OVOCs increased, the concentrations of CO-scaled PAN gradually increased. And when CO-scaled OVOCs concentrations were fixed, as the concentrations of CO-scaled NO_2 increased, PAN did not change significantly. The concentrations of precursors increased largely, which led to the increase of PAN concentrations when $PM_{2.5}$ concentrations elevated. When concentrations of $PM_{2.5}$ were between 75 and 150 $\mu g/m^3$, the concentrations of CO-scaled NO_2 were mainly concentrated in the range of 10-40 ppbv. As the concentrations of CO-scaled OVOCs gradually increased to 15 ppbv, the concentrations of PAN also increased. In addition, there were high concentrations of precursors, which explained the highest daily maximum values and fast generation rate of PAN during this period. Under periods of $PM_{2.5}$ concentrations were between 150 and 250 $\mu g/m^3$, the concentrations of CO-scaled NO_2 mainly changed between 10 ppbv and 60 ppbv. When it was between 10 and 40 ppbv, in the process of the concentrations of CO-scaled OVOCs

rose to 10 ppbv, PAN concentrations also increased. When $PM_{2.5}$ concentrations exceeded 250 μg/m^3, the concentrations of CO-scaled NO_2 decreased, but the concentrations of CO-scaled OVOCs were close. When the CO-scaled NO_2 concentrations were between 10 and 40 ppbv, the PAN concentrations changed significantly with the fluctuation of CO-scaled OVOCs. In particular CO-scaled OVOCs increased from 5 to 10 ppbv, PAN concentrations increased obviously. Apparently, the positive correlation between PAN and precursors concentrations during severe haze period was more obvious. In terms of PAN's relative dependence on its precursors, OVOCs had a greater impact on PAN than NO_2 concentrations did. Especially when the concentrations of NO_2 were between 10 and 40 ppbv, as the concentrations of OVOCs increased, and the concentrations of PAN increased significantly. These results suggested that VOCs emissions made a great contribution to the formation of PAN. Therefore, to reduce PAN pollution, efforts must be made to control VOCs emissions in Wangdu. The sensitivity of PAN to NO_2 enhanced under severely polluted weather which meant the importance of NO_2 control during heavy haze periods.

According to the formation mechanism of PAN, we have discussed solar light intensity and precursors concentrations under different $PM_{2.5}$ concentrations. The results showed that the appropriate light intensity and elevated precursors concentrations generated high concentrations of PAN during haze pollution periods. During haze pollution period, the light intensity and the highest precursors concentrations supported the generation of PAN, especially OVOCs dominated the generation of PAN. In the severe haze pollution periods, the contribution of NO_2 to PAN increased which led to high PAN value and fast formation rate.

2.4. SOA and $PM_{2.5}$

Wangdu experienced severe haze pollution in winter from 2018 to 2019. Measurements at our site showed that the daily average concentrations of $PM_{2.5}$ exceeding 75 μg/m^3 accounted for 85%, with daily maximum breaking through 800 μg/m^3. There are many factors that drive haze pollution, such as traffic emissions, biomass combustion, coal combustion, and secondary aerosols formation. Huang et al. (2014) found that secondary aerosols, i.e., secondary inorganic aerosols (SIA) and secondary organic aerosols (SOA) accounted for 30%-77% for $PM_{2.5}$. Among them, the source apportionment of secondary organic aerosols (SOA) formed from oxidation of VOCs was up to 25%. Especially during heavy pollution periods, $PM_{2.5}$ was mainly composed of secondary components.

Strong secondary generation and regional transmission have been reported to contribute to the increase in $PM_{2.5}$ concentrations (Sun et al., 2019). In order to explore whether active photochemical reaction represented by high concentrations of PAN and the secondary pollutants had an impact on the aggravation of $PM_{2.5}$ concentrations, we selected some periods when the PAN concentrations exceeded 2 ppbv and combined with concentrations of O_3, O_x to conduct detailed analysis. Excluding the explosive growth of $PM_{2.5}$ at nighttime which was considered to be the result of primary emission (Wei et al., 2020), we finally chose four periods (case A:25-27 November; case B: 30 November-3 December; case C: 2-3 January; case D: 4-5 February) To reflect concentration changes controlled by atmospheric chemical process, all data was corrected with CO. The pollutants showed same change patterns in these periods. As shown in the black dashed box in the Fig. 6, during the daytime when photochemical reactions occurred, PAN, O_x, O_3 often started to increase earlier than $PM_{2.5}$. The phenomenon of bimodal interleaving could be observed, which meant that a few hours after the PAN peak appeared, the $PM_{2.5}$ concentration also reached its peak. This phenomenon was in line with the change characteristics that the secondary products of photochemical reactions promoted or initiated the growth of $PM_{2.5}$. At present, laboratory simulation experiments showed that there were heterogeneous reactions on the surface of soot (30-50 nm) which generated CH_3COO^-, $HCOO^-$, NO_3^-, NO_2^-. As the reaction time increased, the proportion of C=O bonds gradually increased which suggested soot was oxidized (Zhao et al., 2017). Kames et al. 1991 noted the hydrolysis mechanism of PAN in water surface. PAN was hydrolyzed to generate organic acids, NO_3^-, NO_2^-. Although the liquid phase reaction of PAN is limited. The real atmospheric environment is complicated, so the liquid phase reaction and particle phase reaction of PAN need more field observations to prove it.

Previous studies have reported several mechanisms of particle growth, including condensation, gas-to-particle partitioning and heterogeneous reaction (Kroll and Seinfeld, 2008; Zhang et al., 2012). Combining previous laboratory simulation results and field observations, it is speculated that PAN may aggravate the haze during the development of the haze. PAN can enter into smaller particles through gas-particle partitioning or condensation and further react to form SOA to promote the growth of PM and aggravate haze pollution. Moreover, the increase of water content in the air during the haze period complicated the PAN heterogeneous reactions. PAN's promotion to PM

concentrations needs more field observations and simulation experiments to support.

3. Conclusions

The study performed continuous field measurements of PAN concentrations combined with supplementary data of $PM_{2.5}$, O_3, O_x, NO, NO_2, photolysis rate constants of NO_2 and O_3 from November 2018 to February 2019 in the rural Wangdu site. The maximum and mean values of PAN concentrations were 4.38 and 0.93±0.67 ppbv in winter, which were at a higher level. In addition to photochemical pollution, Wangdu also experienced severe haze pollution in winter. We focused on the pollution characteristics of PAN, O_3, O_x, NO, NO_2 under different levels of $PM_{2.5}$. Compared with the clean periods, the concentrations of PAN increased significantly during haze periods. Diurnal variation and net formation rate indicated there was the highest daily mean value of 0.64 ppbv and the fastest formation rate of 0.33 ppbv/hr under $PM_{2.5}$ concentrations range of above 250 $\mu g/m^3$. In order to further explain the reasons for the differences under different pollution conditions, we discussed the formation mechanism of PAN. The low temperature contributed to the accumulation of PAN in winter. The photolysis rate constants of NO_2, O_3 showed that the light intensity was not significantly inhibited as $PM_{2.5}$ increased, which was very likely to be the cause of the faster photochemical reaction rate in the haze periods. From the perspective of precursors, the concentrations of OVOCs and NO_2 in the haze period increased obviously. And compared with NO_2, PAN seemed to be more sensitive to changes in OVOCs concentrations, especially when it was low. During the severe haze periods, moderate light intensity and elevated precursors concentrations contributed to the formation of PAN. However, the reason for the different performance of PAN under different $PM_{2.5}$ concentrations during the haze periods which required more field data to explore in the future. In addition, we selected the dates when the PAN exceeded 2 ppbv to analyze the characteristics of PAN, O_3, O_x and $PM_{2.5}$ in detail. As the products of photochemical reactions, PAN, O_3, O_x and $PM_{2.5}$ existed the phenomenon of double peaks staggered. Combining observational data and previous studies on PAN's heterogeneous reactions, we speculate that high concentrations of PAN can aggravate haze pollution by participating in the formation of SOA.

Acknowledgments

This work was supported by the National Natural Science Foundation of China (Nos. 91843301,

91743202, 41805091), Ministry of Science and Technology of China (No. 2016YFC0202700), National research program for key issues in air pollution control (Nos. DQGG0103, DQGG0102) and Marie Skłodowska-Curie Actions (No. 690958-MARSU-RISE-2015).

References

Aikin, A.C., Herman, J.R., Maier, E.J., McQuillan, C.J., 1982. Atmospheric chemistry of ethane and ethylene. J. Geophys. Res.-Oceans 87 (NC4), 3105-3118.

Altshuller, A.P., 1978. Assessment of contribution of chemical species to eye irritation potential of photochemical smog. J. Air Pollut. Control Assoc. 28 (6), 594-598.

Atkinson, R., Baulch, D.L., Cox, R.A., Crowley, J.N., Hampson, R.F., Hynes, R.G., et al., 2004. Evaluated kinetic and photochemical data for atmospheric chemistry: Volume I - gas phase reactions of O_x, HO_x, NO_x and SO_x species. Atmos. Chem. Phys. 4, 1461-1738.

Atkinson, R., Baulch, D.L., Cox, R.A., Hampson, R.F., Kerr, J.A., Rossi, M.J., et al., 1997. Evaluated kinetic, photochemical and heterogeneous data for atmospheric chemistry: Supplement V. IUPAC subcommittee on gas kinetic data evaluation for atmospheric chemistry. J. Phys. Chem. Ref. Data 26 (3), 521-1011.

Atkinson, R., Baulch, D.L., Cox, R.A., Jr., R.F.H., Kerr, J.A., Troe, J., 1992. Evaluated kinetic and photochemical data for atmospheric chemistry: Supplement IV. IUPAC subcommittee on gas kinetic data evaluation for atmospheric chemistry. J. Phys. Chem. Ref. Data 21 (6), 1125-1568.

Bao, F.X., Li, M., Zhang, Y., Chen, C.C., Zhao, J.C., 2018. Photochemical Aging of Beijing Urban $PM_{2.5}$: HONO Production. Environ. Sci. Technol. 52 (11), 6309-6316.

Carter, W.P.L., Winer, A.M., Pitts, J.N., 1981. Effect of peroxyacetyl nitrate on the initiation of photochemical smog. Environ. Sci. Technol. 15 (7), 831-834.

Casasanta, G., di Sarra, A., Meloni, D., Monteleone, F., Pace, G., Piacentino, S., et al., 2011. Large aerosol effects on ozone photolysis in the Mediterranean. Atmos. Environ. 45 (24), 3937-3943.

Frenzel, A., Kutsuna, S., Takeuchi, K., Ibusuki, T., 2000. Solubility and reactivity of peroxyacetyl nitrate (PAN) in dilute aqueous salt solutions and in sulphuric acid. Atmos. Environ. 34 (21), 3641-3644.

Fuchs, H., Tan, Z.F., Lu, K.D., Bohn, B., Broch, S., Brown, S.S., et al., 2017. OH reactivity at a rural site (Wangdu) in the North China Plain: contributions from OH reactants and experimental OH budget. Atmos. Chem. Phys. 17 (1), 645-661.

Gaffney, J.S., Marley, N.A., Cunningham, M.M., Doskey, P.V., 1999. Measurements of peroxyacyl nitrates (PANs) in Mexico City: implications for megacity air quality impacts on regional scales. Atmos. Environ. 33 (30), 5003-5012.

Grosjean, E., Grosjean, D., Woodhouse, L.F., 2001. Peroxyacetyl nitrate and peroxypropionyl nitrate during SCOS97-NARSTO. Environ. Sci. Technol. 35 (20), 4007-4014.

Han, J., Lee, M., Shang, X., Lee, G., Emmons, L.K., 2017. Decoupling peroxyacetyl nitrate from ozone in Chinese outflows observed at Gosan Climate Observatory. Atmos. Chem. Phys. 17 (17), 10619-10631.

Honrath, R.E., Hamlin, A.J., Merrill, J.T., 1996. Transport of ozone precursors from the Arctic troposphere to the North Atlantic region. J. Geophys. Res.-Atmos. 101 (D22), 29335-29351.

Hu, B., Liu, T., Hong, Y., Xu, L., Li, M., Wu, X., et al., 2020. Characteristics of peroxyacetyl nitrate (PAN) in a coastal city of southeastern China: photochemical mechanism and pollution process. Sci. Total Environ. 719, 137493.

Huang, R.J., Zhang, Y.L., Bozzetti, C., Ho, K.F., Cao, J.J., Han, Y.M., et al., 2014. High secondary aerosol

contribution to particulate pollution during haze events in China. Nature 514 (7521), 218-222.
Jacobi, H.W., Weller, R., Bluszcz, T., Schrems, O., 1999. Latitudinal distribution of peroxyacetyl nitrate (PAN) over the Atlantic Ocean. J. Geophys. Res.-Atmos. 104 (D21), 26901-26912.
Kames, J., Schweighoefer, S., Schurath, U., 1991. Henry's law constant and hydrolysis of peroxyacetyl nitrate (PAN). J. Atmos. Chem. 12 (2), 169-180.
Kondo, T., Taniguchi, M., Shibano, M., Wang, N.H., Baba, K., 2008. Coumarins from the roots of Ligusticum multivittatum. J. Nat. Med. 62 (1), 87-90.
Kroll, J.H., Seinfeld, J.H., 2008. Chemistry of secondary organic aerosol: Formation and evolution of low-volatility organics in the atmosphere. Atmos. Environ. 42 (16), 3593-3624.
Kuang, Y., He, Y., Xu, W., Yuan, B., Zhang, G., Ma, Z., et al., 2020. Photochemical aqueous-phase reactions induce rapid daytime formation of oxygenated organic aerosol on the North China Plain. Environ. Sci. Technol. 54 (7), 3849-3860.
LaFranchi, B.W., Wolfe, G.M., Thornton, J.A., Harrold, S.A., Browne, E.C., Min, K.E., et al., 2010. Closing the Peroxy Acetyl (PA) Radical Budget: Observations of Acyl Peroxy Nitrates (PAN, PPN, and MPAN) During BEARPEX 2007, in: Steyn D.G., Rao S.T. (Eds.), Air Pollution Modeling and Its Application Xx. Springer: Dordrecht, pp. 255-256.
Langer, S., Wangberg, I., Ljungstrom, E., 1992. Heterogeneous transformation of peroxyacetylnitrate . Atmos. Environ. Part A. General Top. 26 (17), 3089-3098.
Lee, J.-B., Yoon, J.-S., Jung, K., Eom, S.-W., Chae, Y.-Z., Cho, S.-J., et al., 2013. Peroxyacetyl nitrate (PAN) in the urban atmosphere. Chemosphere 93 (9), 1796-1803.
Liu, C.T., Ma, Z.B., Mu, Y.J., Liu, J.F., Zhang, C.L., Zhang, Y.Y., et al., 2017. The levels, variation characteristics, and sources of atmospheric non-methane hydrocarbon compounds during wintertime in Beijing, China. Atmos. Chem. Phys. 17 (17), 10633-10649.
Liu, L., Wang, X., Chen, J., Xue, L., Wang, W., Wen, L., et al., 2018. Understanding unusually high levels of peroxyacetyl nitrate (PAN) in winter in Urban Jinan, China. J. Environ. Sci. 71, 249-260.
Liu, P.F., Zhang, C.L., Xue, C.Y., Mu, Y.J., Liu, J.F., Zhang, Y.Y., et al., 2017. The contribution of residential coal combustion to atmospheric $PM_{2.5}$ in northern China during winter. Atmos. Chem. Phys.17 (18), 11503-11520.
Liu, Z., Hu, B., Ji, D., Cheng, M., Gao, W., Shi, S., et al., 2019. Characteristics of fine particle explosive growth events in Beijing, China: seasonal variation, chemical evolution pattern and formation mechanism. Sci. Total Environ. 687, 1073-1086.
Liu, Z., Wang, Y.H., Costabile, F., Amoroso, A., Zhao, C., Huey, L.G., et al., 2014. Evidence of aerosols as a media for rapid daytime HONO production over China. Environ. Sci. Technol. 48 (24), 14386-14391.
Lu, K.D., Hofzumahaus, A., Holland, F., Bohn, B., Brauers, T., Fuchs, H., et al., 2013. Missing OH source in a suburban environment near Beijing: observed and modelled OH and HO_2 concentrations in summer 2006. Atmos. Chem. Phys. 13 (2), 1057-1080.
Mills, G.P., Sturges, W.T., Salmon, R.A., Bauguitte, S.J.B., Read, K.A., Bandy, B.J., 2007. Seasonal variation of peroxyacetylnitrate (PAN) in coastal Antarctica measured with a new instrument for the detection of sub-part per trillion mixing ratios of PAN. Atmos. Chem. Phys. 7 (17), 4589-4599.
Orlando, J.J., Tyndall, G.S., Calvert, J.G., 1992. Thermal-decomposition pathways for peroxyacetyl nitrate (PAN) - implications for atmospheric methyl nitrate levels. Atmos. Environ. Part A. General Top. 26 (17), 3111-3118.
Roberts, J.M., Flocke, F., Chen, G., de Gouw, J., Holloway, J.S., Hubler, G., et al., 2004. Measurement of peroxycarboxylic nitric anhydrides (PANs) during the ITCT 2K2 aircraft intensive experiment. J.

Geophys. Res.-Atmos. 109 (D23), 13.
Singh, H.B., Salas, L.J., 1983. Peroxyacetyl nitrate in the free troposphere. Nature 302 (5906), 326-328.
Singh, H.B., Salas, L.J., Viezee, W., 1986. Global distribution of peroxyacetyl nitrate. Nature 321 (6070), 588-591.
Stephens, E.R., Hanst, P.L., Doerr, R.C., Scott, W.E., 1956. Reactions of nitrogen dioxide and organic compounds in air. Ind. Eng. Chem. 48 (9), 1498-1504.
Sun, J., Wu, F.K., Hu, B., Tang, G.Q., Zhang, J.K., Wang, Y.S., 2016. VOC characteristics, emissions and contributions to SOA formation during hazy episodes. Atmos. Environ. 141, 560-570.
Sun, J.J., Liang, M.J., Shi, Z.H., Shen, F.Z., Li, J.Y., Huang, L., et al., 2019. Investigating the $PM_{2.5}$ mass concentration growth processes during 2013-2016 in Beijing and Shanghai. Chemosphere 221, 452-463.
Sun, M., Cui, J.n., Zhao, X., Zhang, J., 2020. Impacts of precursors on peroxyacetyl nitrate (PAN) and relative formation of PAN to ozone in a southwestern megacity of China. Atmos. Environ. 231, 117542.
Taylor, O.C., 1969. Importance of peroxyacetyl nitrate (PAN) as a phytotoxic air pollutant. J. Air Pollut. Control Assoc. 19 (5), 347-351.
Villalta, P.W., Howard, C.J., 1996. Direct kinetics study of the $CH3C(O)O_2$ + NO reaction using chemical ionization mass spectrometry. J. Phys. Chem. 100 (32), 13624-13628.
Wang, B., Shao, M., Roberts, J.M., Yang, G., Yang, F., Hu, M., et al., 2010. Ground-based on-line measurements of peroxyacetyl nitrate (PAN) and peroxypropionyl nitrate (PPN) in the Pearl River Delta, China. Int. J. Environ. Anal. Chem. 90 (7), 548-559.
Wei, Y., Chen, H., Sun, H., Zhang, F., Shang, X., Yao, L., et al., 2020. Nocturnal $PM_{2.5}$ explosive growth dominates severe haze in the rural North China Plain. Atmos. Res. 242, 105020.
Xu, Q.C., Wang, S.X., Jiang, J.K., Bhattarai, N., Li, X.X., Chang, X., et al., 2019. Nitrate dominates the chemical composition of PM2.5 during haze event in Beijing, China. Sci. Total Environ. 689, 1293-1303.
Xu, X.B., Zhang, H.L., Lin, W.L., Wang, Y., Xu, W.Y., Jia, S.H., 2018. First simultaneous measurements of peroxyacetyl nitrate (PAN) and ozone at Nam Co in the central Tibetan Plateau: impacts from the PBL evolution and transport processes. Atmos. Chem. Phys. 18 (7), 5199-5217.
Xue, L., Wang, T., Wang, X., Blake, D.R., Gao, J., Nie, W., et al., 2014. On the use of an explicit chemical mechanism to dissect peroxy acetyl nitrate formation. Environ. Pollut. 195, 39-47.
Zeng, L., Fan, G.-J., Lyu, X., Guo, H., Wang, J.-L., Yao, D., 2019. Atmospheric fate of peroxyacetyl nitrate in suburban Hong Kong and its impact on local ozone pollution. Environ. Pollut. 252, 1910-1919.
Zhang, G., Mu, Y.J., Liu, J.F., Zhang, C.L., Zhang, Y.Y., Zhang, Y.J., et al., 2014. Seasonal and diurnal variations of atmospheric peroxyacetyl nitrate, peroxypropionyl nitrate, and carbon tetrachloride in Beijing. J. Environ. Sci. 26 (1), 65-74.
Zhang, G., Xia, L., Zang, K., Xu, W., Zhang, F., Liang, L., et al., 2020. The abundance and inter-relationship of atmospheric peroxyacetyl nitrate (PAN), peroxypropionyl nitrate (PPN), O_3, and NO_y during the wintertime in Beijing, China. Sci. Total Environ. 718, 137388.
Zhang, J.M., Wang, T., Ding, A.J., Zhou, X.H., Xue, L.K., Poon, C.N., et al., 2009. Continuous measurement of peroxyacetyl nitrate (PAN) in suburban and remote areas of western China. Atmos. Environ. 43 (2), 228-237.
Zhang, J.W., Chen, J.M., Xue, C.Y., Chen, H., Zhang, Q., Liu, X.G., et al., 2019. Impacts of six potential HONO sources on HO_x budgets and SOA formation during a wintertime heavy haze period in the North China Plain. Sci. Total Environ. 681, 110-123.
Zhang, Q., Quan, J., Tie, X., Li, X., Liu, Q., Gao, Y., et al., 2015. Effects of meteorology and secondary particle formation on visibility during heavy haze events in Beijing, China. Sci. Total Environ. 502, 578-

584.
Zhang, R.Y., Khalizov, A., Wang, L., Hu, M., Xu, W., 2012. Nucleation and Growth of Nanoparticles in the Atmosphere. Chem. Rev. 112 (3), 1957-2011.
Zhao, X.M., Gao, T.Y., Zhang, J.B., 2017. Heterogeneous reaction of peroxyacetyl nitrate (PAN) on soot. Chemosphere 177, 339-346.
Zhu, H., Gao, T., Zhang, J., 2018. Wintertime characteristic of peroxyacetyl nitrate in the Chengyu district of southwestern China. Environ. Sci. Pollut. Res. 25 (23), 23143-23156.

Table 1 Summary of PAN concentrations in other studies.

Location	Site description	Monitoring time	PAN (ppbv)		References
			Maximum values	Mean values	
Wangdu, China	Rural	November 2018-March 2019	4.48	0.78±0.66	This study
Ziyang, China	Urban	December 2012	1.61	0.55	Zhu et al., 2018
Jinan, China	Urban	November 2015-January 2016	9.61	1.89±1.42	Liu et al., 2018
Beijing, China	Urban	November 2012-January 2013	1.46	0.31	Zhang et al., 2020
Xiamen, China	Urban	December 2017-February 2018	4.19	0.64	Hu et al., 2020
Hong Kong, China	Suburban	October-December 2016	7.30	0.63±0.05	Zeng et al., 2019
Beijing, China	Urban	July-August 2008	9.34		Xue et al., 2014
Chongqing, China	Urban	August-September 2015	12.17	2.05±0.94	Sun et al., 2020
Pearl River Delta Region, China	Suburban	November-December 2011	2.80	0.69±0.46	Wang et al., 2010
Tibetan Plateau, China	Rural	August 2011	0.76	0.36	Xu et al., 2018
		May-July 2012	0.99	0.44	
Seoul, Korea	Urban	Winter 2011	5.03	0.64±0.49	Lee et al., 2013
Jeju Island, Korea	Rural	October-November 2010	2.40	0.60	Han et al., 2017
Azusa, USA	Rural	July-October 1997	4.84	0.88±0.74	Grosjean et al., 2001
Simi Valley, USA	Rural	June-October 1997	2.99	0.61±0.43	
Mexico, USA	Urban	February-March 1997	34		Gaffney et al., 1999

Table 2 Lifetime and reaction rate (k) of PAN under different conditions.

Condition	k_2 ($\times 10^{-11}$ cm^3/(molecule·sec))	k_3 ($\times 10^{-6}$ sec^{-1})	k_4 ($\times 10^{-11}$ cm^3/(molecule·sec))	Temperature (K)	NO_2/NO	Lifetime (days)
Clean days	1.32	4.42	2.21	269	50.04	80
Moderate haze days	1.30	7.72	2.18	272	10.31	10
Severe haze days	1.30	9.27	2.17	273	4.49	5

Reaction rate constants for Reactions (4, 5, 6) (k_2. k_3. k_4) refer to the references Atkinson et al., 1997; Villalta and Howard, 1996

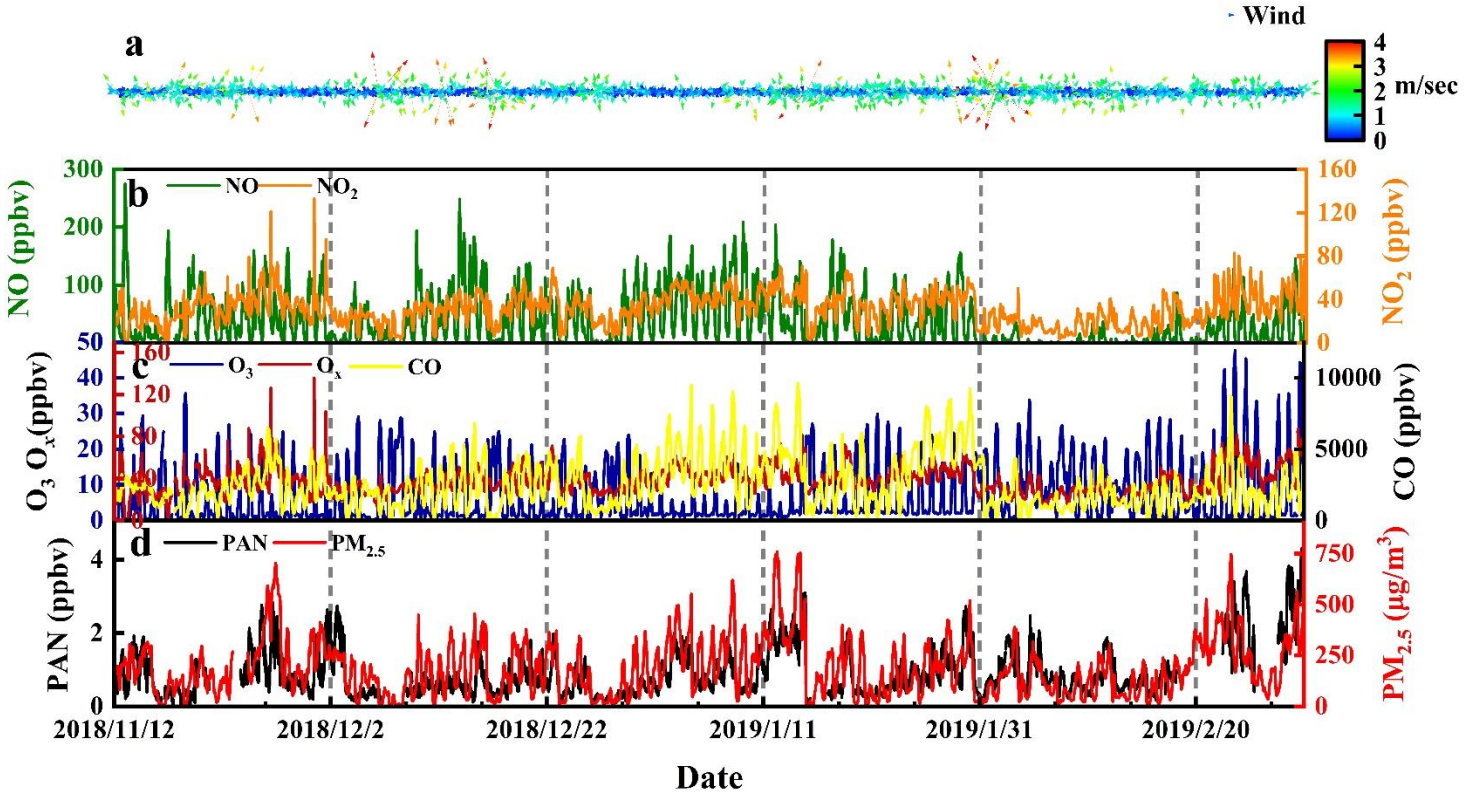

Fig. 1 Time series of pollutants and meteorological parameters in Wangdu between November 2018 and February 2019. (a) wind direction and wind speed; (b) NO, NO_2; (c) O_3, O_x, CO; (d) peroxyacetyl nitrate (PAN), $PM_{2.5}$.

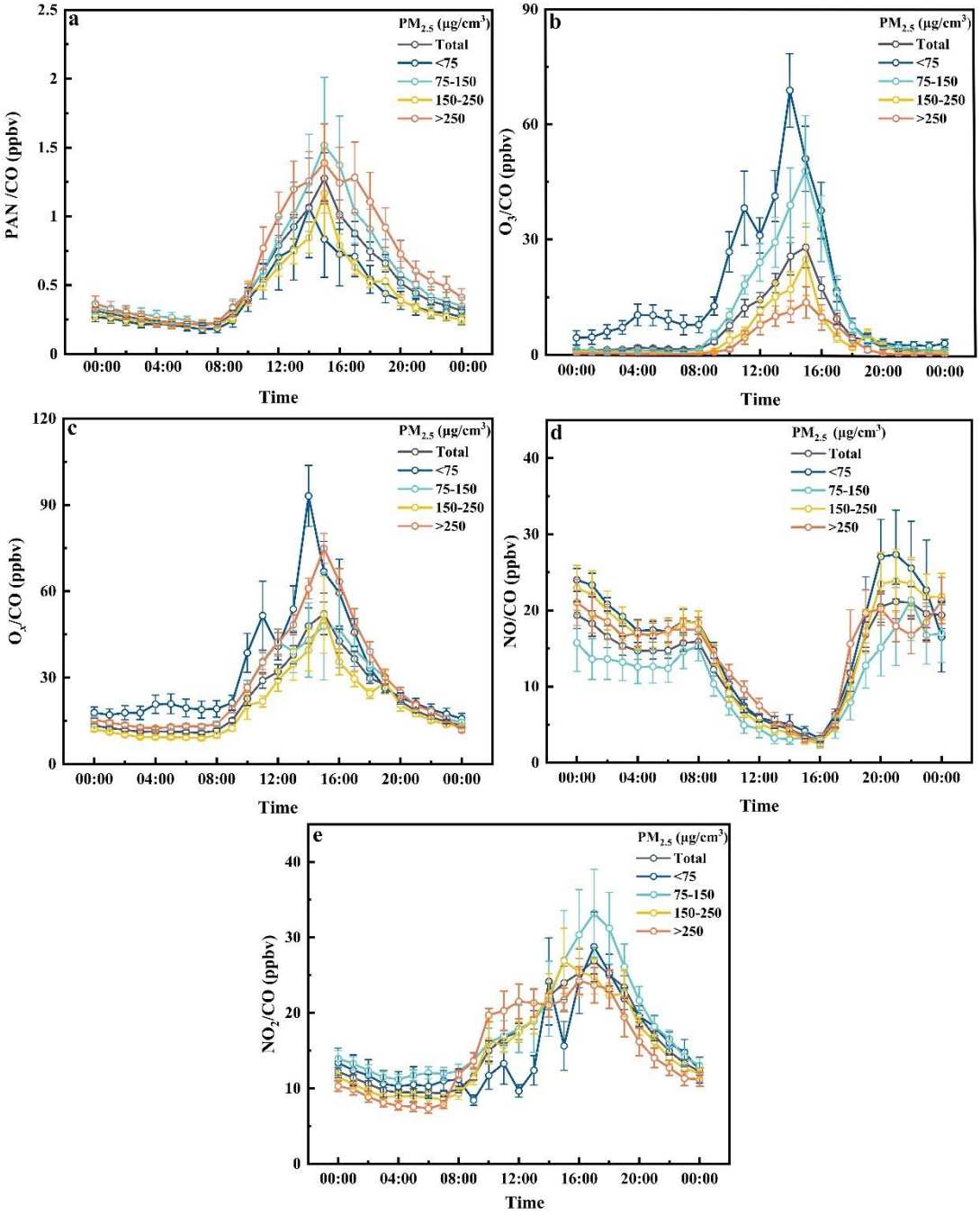

Fig. 2 Diurnal variation of (a) PAN, (b) O_3, (c) O_x, (d) NO, and (e) NO_2 under different concentrations of $PM_{2.5}$. Error bars are standard errors.

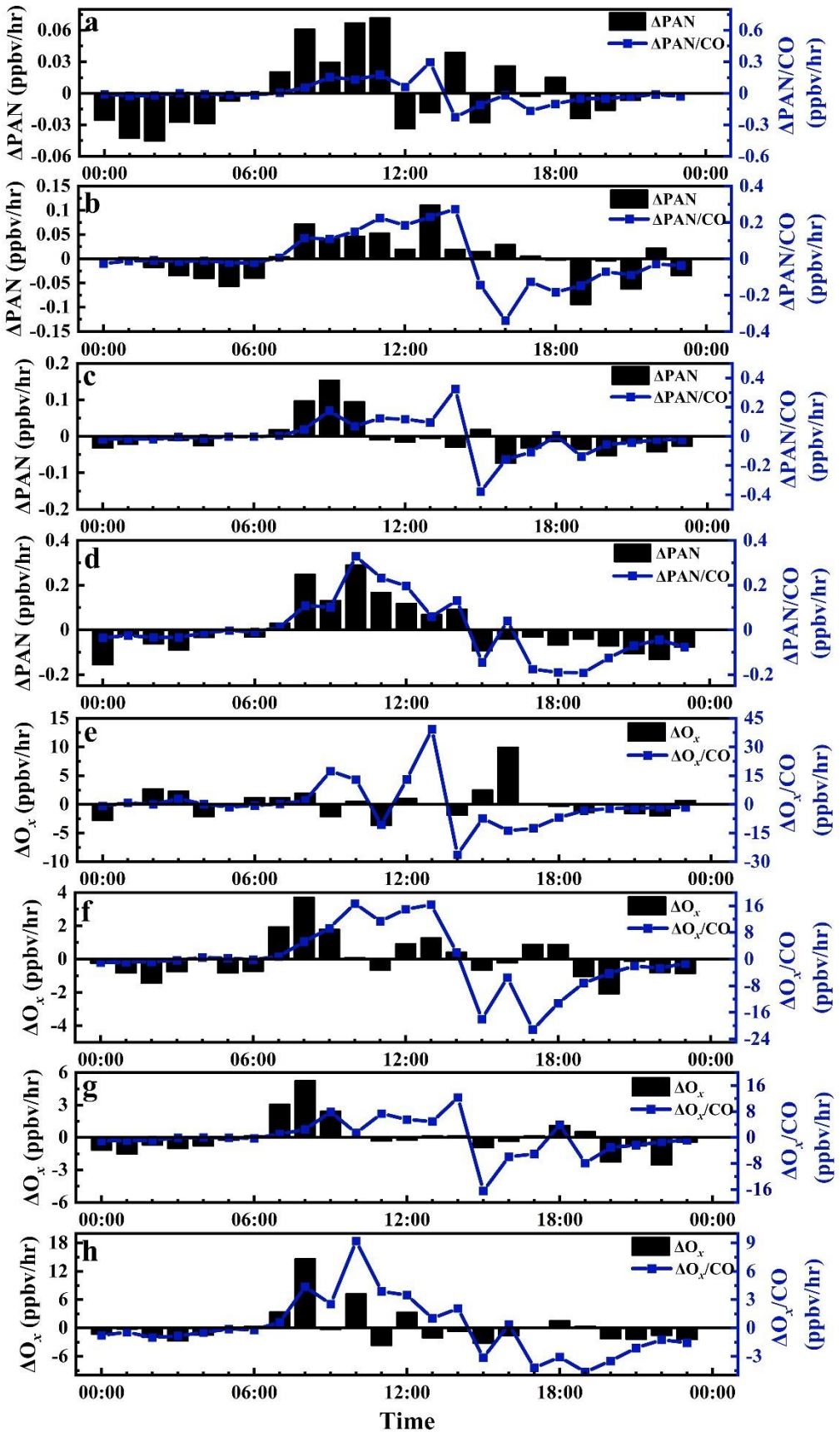

Fig. 3 Generation rate of PAN and O_x (ΔPAN and ΔO_x) under different concentrations of $PM_{2.5}$:

(a,e) <75 μg/cm^3, (b,f) 75-150 μg/cm^3, (c,g) 150-250 μg/cm^3 and (d,h) >250 μg/cm^3.

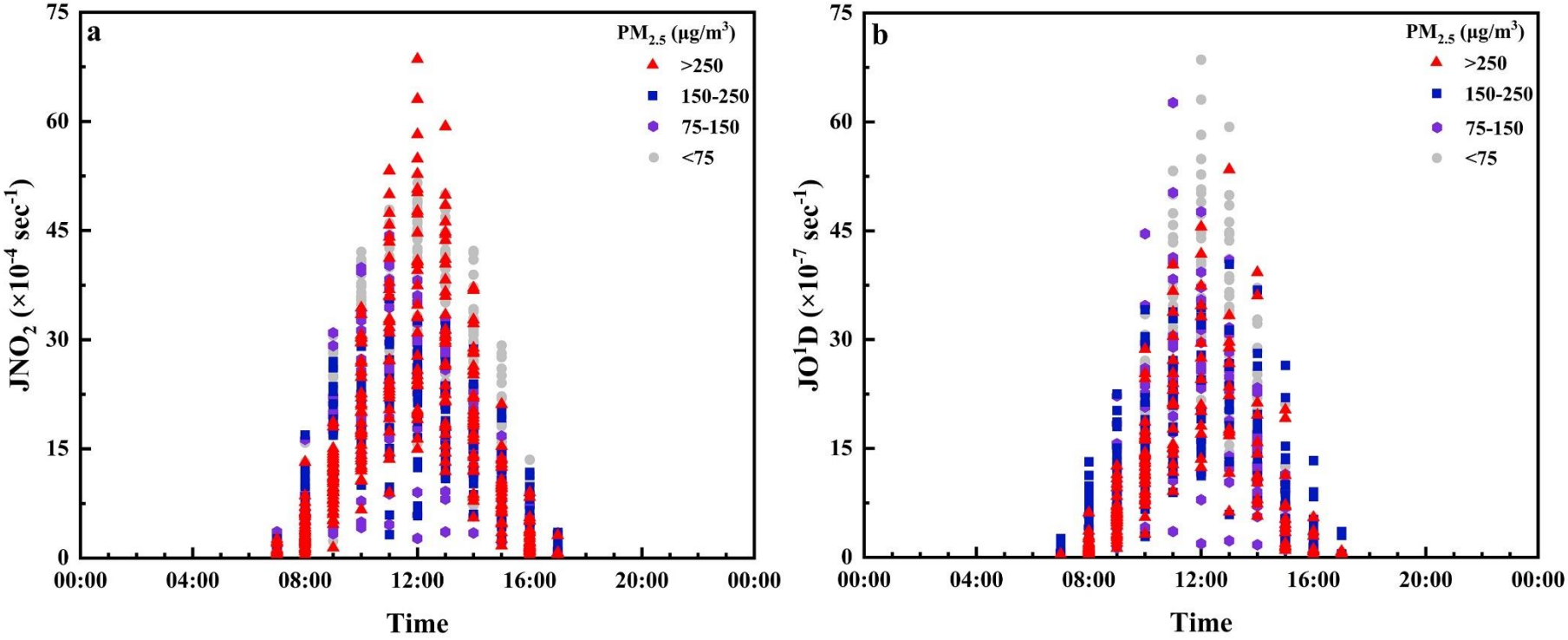

Fig. 4 Diurnal variation in the photolysis rate constants of NO_2 ($J(NO_2)$) and O_3 ($J(O^1D)$) color-coded by different concentrations of $PM_{2.5}$

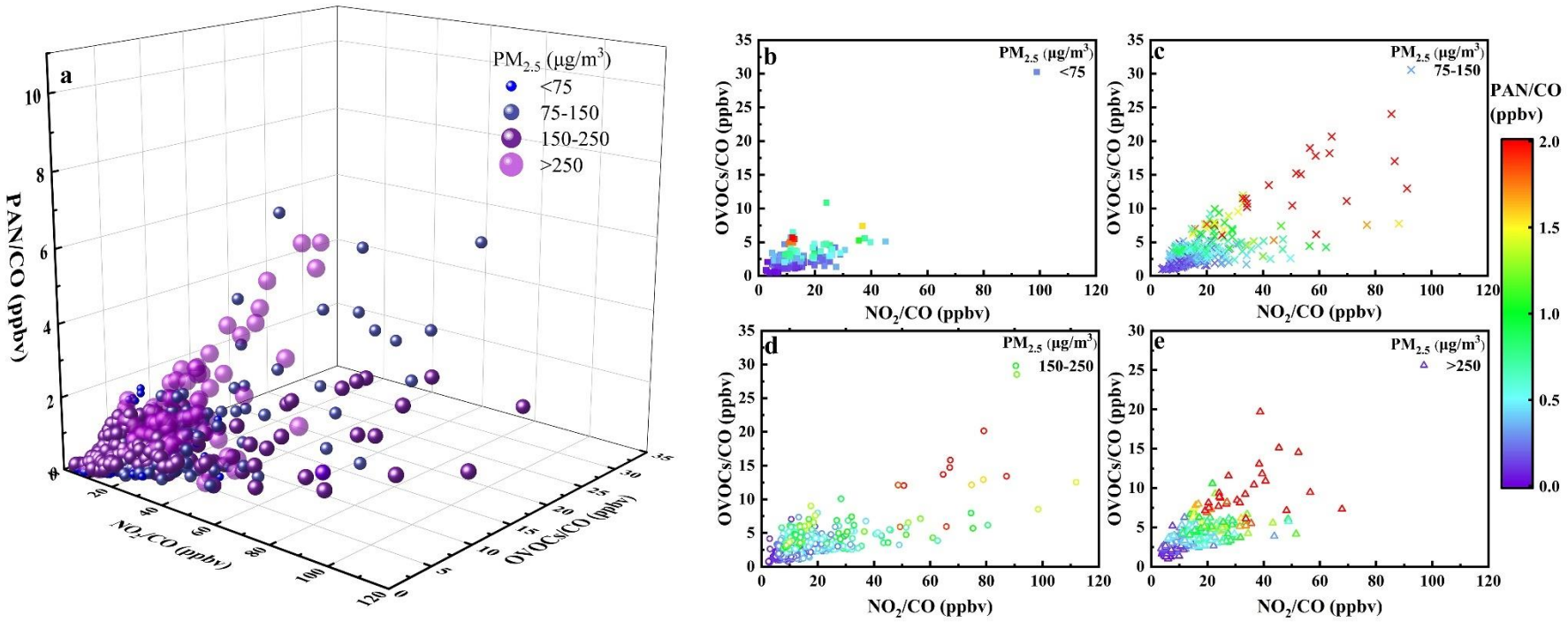

Fig. 5 Relationship of PAN and its precursors NO_2, oxygenated volatile organic compounds (OVOCs) under different concentrations of PAN: (a) overall 3D scatter plot, (b) < 75 μg/cm^3, (c) 75-150 μg/cm^3, (d) 150-250 μg/cm^3 and (d) >250 μg/cm^3.

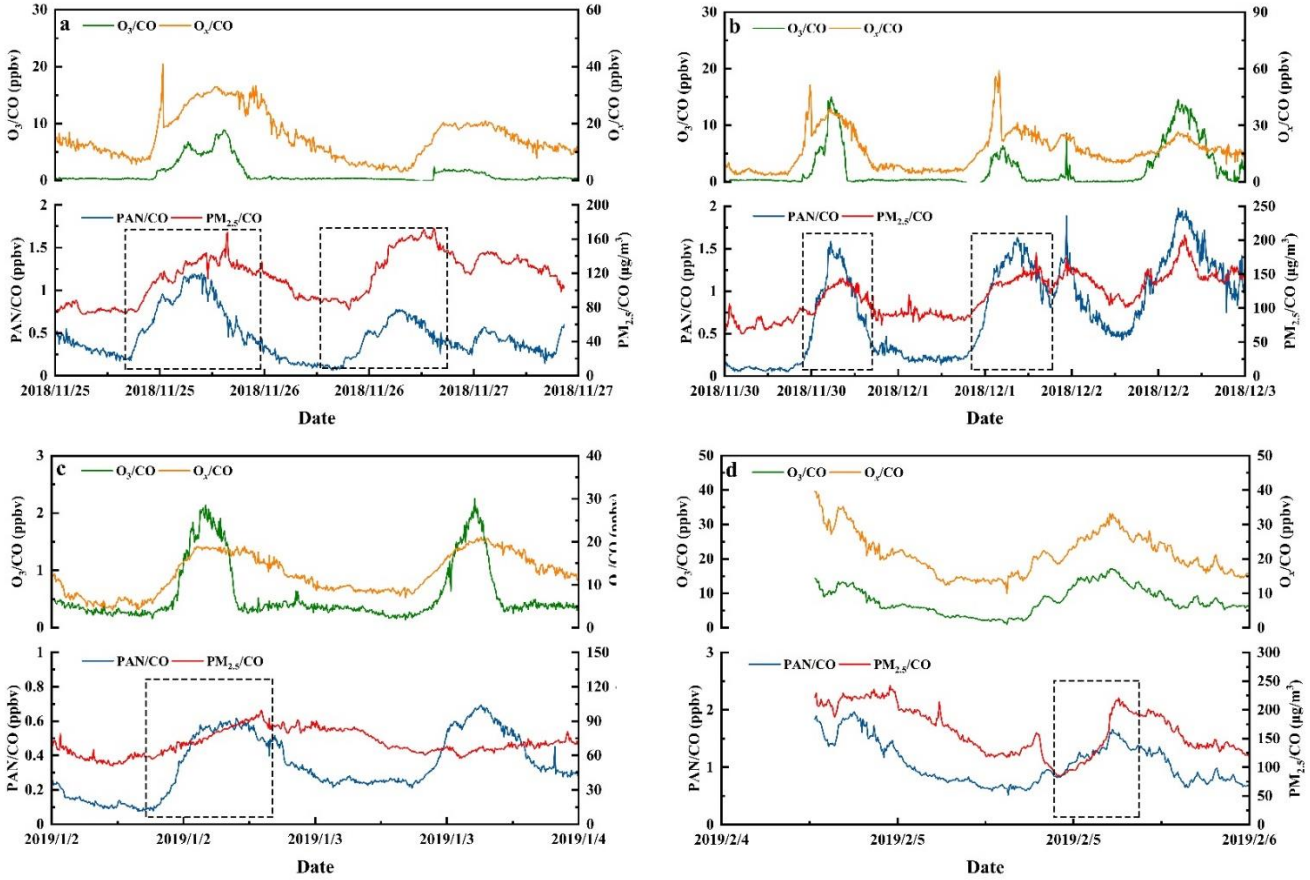

Fig. 6 Diurnal cycles of PAN, $PM_{2.5}$, O_3, and O_x on case (a) 25-27 November, 2018, (b) 30 November, 2018-2 December, 2018, (c) 2-3 January, 2019; (d) 4-5 February, 2019.